ISSN 0915-633X

NATIONAL INSTITUTE FOR FUSION SCIENCE

Long-pulse Operation of a Cesium-Seeded High-Current Large Negative Ion Source

Y. Takeiri, M. Osakabe, Y. Oka, K. Tsumori, O. Kaneko,
T. Takanashi, E. Asano, T. Kawamoto,
R. Akiyama and T. Kuroda

(Received - Dec. 12, 1996)

NIFS-476 Jan. 1997

RESEARCH REPORT
NIFS Series

NAGOYA, JAPAN

Long-pulse operation of a cesium-seeded high-current large negative ion source

Y. Takeiri, M. Osakabe, Y. Oka, K. Tsumori, O. Kaneko, T. Takanashi,
E. Asano, T. Kawamoto, R. Akiyama, and T. Kuroda

National Institute for Fusion Science, Nagoya 464-01, Japan

ABSTRACT

A high-power large negative ion source has been operated for a long pulse duration. A three-grid single-stage accelerator is used, where the extraction grid is shaped so that the secondary electrons generated on the extraction grid would be prevented from leaking into the acceleration gap. A stable long-pulse arc discharge with an arc power of 100 kW has been obtained over 15 s by balancing an individual arc current flowing through each filament. The cesium-seeded operation is not influenced by a temperature rise of over 100 ℃ of the plasma grid during the long-pulse arc discharge. As a result, the negative ion beam power of 330 kW (91 keV-3.6 A) was produced stably for 10 s from an area of 25 cm × 26 cm, where the current density was 21 mA/cm^2 and the negative ion power density was 1.9 kW/cm^2. The neutralization efficiency of accelerated negative ions has been measured including the residual positive and negative ion ratios by the water calorimetry of the beam dumps. The result agrees well with the calculation result.

Keywords : negative ion source, negative-ion-based NBI, long pulse operation, cesium seeding, long-pulse arc discharge, grid thermal load, neutralization efficiency, grid aperture shaping, stripping loss

I. INTRODUCTION

In the next step experimental fusion devices, such as ITER (International Tokamak Experimental Reactor),[1] high-energy and long-pulse neutral beam injection (NBI) heating is projected.[2] For this purpose, high-power large negative ion sources have been intensively developed in various laboratories.[3-5] As a result, a high-current H^- ion beam of 16.2 A was produced at NIFS [6] and 13.5 A of D^- ions was accelerated to 400 keV at JAERI.[7] Recently, the first injection to JT60U tokamak using a negative-ion-based NBI system has been reported.[8] However, these results were obtained in a short-pulse operation below 0.3 s. In the Large Helical Device (LHD) project,[9] the pulse duration of a negative-ion-based NBI system, which is now under construction, is planned to be 10 s.[10,11] Therefore, a long-pulse operation over 10 s should be achieved with a high-power large negative ion source.

There are several key issues to be solved for the long-pulse operation of the high-power large negative ion source. Since the ion source is operated with cesium seeded for the enhancement of the negative ion current and the lowering of the operational gas pressure, the operation stability and reliability are important for the long-pulse operation. Using a cylindrical negative ion source of 20 cm in diameter, a long-pulse operation of 1000 s was demonstrated in a cesium-seeded operation with a H^- ion beam power of 25 kW (50 keV-0.5 A).[12] It is required that a higher-power negative ion beam is produced for a long-pulse duration in a large negative ion source. A long-pulse stable arc discharge is also important. The volume negative ion source utilizes the cusp magnetic field and the magnetic filter field, and these magnetic fields distribute in the arc chamber. Moreover, for improvement of the negative ion production efficiency in a low gas pressure, these magnetic fields are strong. In this situation, it is not easy that a high-power arc discharge is maintained stably for a long period in a large arc chamber. The most significant problem is the thermal load of grids. In the negative ion source, the negative ions accompany the electrons, which are accelerated together with the negative ions and lead to the thermal load of the downstream grid. The suppression of the accelerated electrons has been investigated,[13] and the low gas pressure operation is quite important to reduce the detached electrons generated by the negative ion stripping during the acceleration.

We developed a large hydrogen negative ion source, which produced 16.2 A of the negative ions, and have modified it for the long-pulse operation. As a result, a long-pulse operation of 10 s was achieved with a beam power of 330 kW. In this paper, after the description of the negative ion source, the experimental results of the long-pulse operation are presented from points of view of the long-pulse stable arc discharge, the operational stability of the negative ion beam properties against the pulse duration, and the thermal loads of the grids.

The high-power long-pulse negative ion beam production for 10 s is demonstrated. The neutralization efficiency measured calorimetrically with beam dumps is also described.

II. EXPERIMENTAL APPARATUS

A. External filter type large negative ion source

A schematic diagram of an external filter type large negative ion source [4,6,14,15] is shown in Fig. 1. An arc chamber is made of copper, the dimensions of which are 35 cm × 62 cm in cross section and 19 cm in depth. To improve the plasma confinement, strong cusp magnetic field is configured, whose strength is about 1.8 kG on the chamber inner surface. Tungsten filaments of 1.8 mm in diameter are used for filament-arc discharge. Permanent magnets of Nd-Fe-B are contained in a filter flange made of copper, and generate a strong external magnetic filter field in a wide area of 35 cm × 62 cm in front of the plasma grid. The central magnetic filter field strength is 52 G and the line-integrated field strength is 650 G cm. Two cesium ovens are installed on the side wall of the arc chamber. The arc chamber, the filament feedthroughs and the filter flange are water-cooled for long-pulse arc discharge.

The negative ion accelerator consists of plasma grid, extraction grid and grounded grid, as shown in Fig. 2. Two types of accelerator are used in the experiments. One is with a straight aperture extraction grid as shown in Fig. 2 (a), and the other is with a shaped aperture extraction grid as shown in Fig. 2 (b). The latter accelerator prevents the secondary electrons generated on the extraction grid from being accelerated, leading to the smaller thermal load of the grounded grid than that in the former accelerator.[13] The accelerator with the straight aperture extraction grid is used in a short pulse operation below 1 s, and that with the shaped aperture extraction grid is used in a long pulse operation over 1 s. The plasma grid, made of molybdenum, has 270 apertures of 9 mm in diameter in an area of 25 cm × 26 cm. The extraction grid, made of copper, contains permanent magnets for the electron suppression and is cooled with the buried copper water cooling tubes. The grounded grid, which suffers high thermal load, is made of copper and water-cooled with silver-soldered copper tubes of 4 mm in outer diameter. The thermal loads of the extraction grid and the grounded grid are estimated by the water-calorimetry, where the temperature rise of the cooling water and the water flow rate are measured. The multibeamlets are focused around 12 m downstream by the aperture displacement of the grounded grid.[15] The maximum extraction and acceleration voltages are 9 kV and 90 kV, respectively.

The negative ion current is measured with two calorimeter arrays located 5 m and 11.2 m downstream from the ion source when the pulse duration is below 1 s. The maximum pulse

duration is limited to 10 s by specification of the power supplies.

B. Negative-ion-based NBI teststand

The negative ion source is installed to a negative-ion-based NBI teststand [16,17] via a gate valve of 800 mm in diameter, as shown in Fig. 3. The teststand has two large vacuum vessels — the ion source vacuum vessel and the beam dump vacuum vessel, which are connected through a 5-m long neutralizer. A cryopump system with a pumping speed of 450 m^3/s is installed in the ion source vessel. The beam passing through the neutralizer consists of the neutral beam and the positive and the negative ion beams. The neutral beam is incident on a neutral beam dump, and the positive and the negative ion beams are deflected by an ion deflecting magnet and incident on a positive and a negative ion beam dumps, respectively. The beam dumps are made of swirl tubes and withstand 1.6 kW/cm^2 of the thermal load continuously. The calorimeter arrays 5 m and 11.2 m downstream are located at the entrance and the exit of the neutralizer, respectively.

III. EXPERIMENTAL RESULTS AND DISCUSSION

A. Long-pulse arc discharge

The external magnetic filter is distributed over a wide area and the field-free region is narrow in the arc chamber. Moreover, as the cusp magnetic field is strong, the anode area is also small. In this situation, which is required for the efficient negative ion production, the arc discharge tends to be inhomogeneous and sometimes results in the local run-away of discharge especially in a low gas pressure operation. Although the magnetic filter field should be homogenized, uniformity of an individual arc current flowing through each filament is important to suppress the local run-away of discharge. The filament power supply provides eight electrically isolated outputs, and a variable resistance is inserted between the individual isolated filament power supply output and the arc power supply, as shown in Fig. 4 (a). The individual arc current flowing through each filament can be controlled by adjusting the variable resistance.

An example of the individual arc current distribution is shown in Fig. 4 (b). There are 12 filaments inserted from the side wall, 8 from longer sides (#3 - 6 and #9 - 12) and 4 from shorter sides (#1, 2, 7 and 8), and 6 isolated filament power supply outputs are used, each of which is connected to 2 filaments. Although the time evolution of the individual arc current is not the same for each filament, all the individual arc currents reach a steady state and are around 100 A in about 5 s after the start of discharge. By this method, a long-pulse arc discharge of 15

s has been stably obtained with a total arc power of more than 100 kW. It has been reported that the method of inserting the variable resistance is effective for making the plasma uniform in a large negative ion source.[18] Therefore, the balanced distribution of the individual arc current would lead to a uniform plasma production.

B. Negative ion beam properties in long-pulse arc discharges

The negative ion source is operated with continuous cesium seeding at a rather low rate, where the cesium reservoir temperature is around 170 ℃. The steady-state arc discharge is obtained in 5 s, and it is important to investigate the negative ion beam properties in a long-pulse stable arc discharge. Figure 5 shows the H^- ion current, I_{H^-}, the extraction current, I_{ext}, and the acceleration current, I_{acc}, as a function of the pulse length in a long-pulse arc discharge. The FWHM of the vertical profile of the H^- ion beam is also shown in Fig. 5. The arc power is 60 kW. The currents and the beam profile are not changed by the pulse length variation below 1 s.

The I_{H^-}, I_{ext}, I_{acc} and the 1/e-half width of the vertical profile of the H^- ion beam are shown in Fig. 6, as a function of the plasma grid temperature. The arc power is 67 kW and the pulse length is 0.6 s. The currents and the beam profile are insensitive to the plasma grid temperature variation of 180-300 ℃. In the short-pulse arc discharge, the cesium effects such as the enhancement of the H^- ion current and the reduction of the extraction current are dependent on the plasma grid temperature, and the higher plasma grid temperature leads to the more H^- ion current and the less extraction current.[19,20] The plasma grid temperature dependence has been explained by the surface production of the negative ions on the cesium-covered plasma grid, which has a low work function. The binding energy of the cesium to the substrate surface is large and that of the cesium to the cesium layer is small. Therefore, a half- to mono-layer of the cesium coverage, where the work-function is almost the minimum, is formed by raising the plasma grid temperature, resulting in the enhancement of the negative ion current. However, the plasma grid temperature dependence disappears in a long-pulse arc discharge, as shown in Fig. 6. The injected cesium, which is adsorbed on the cold chamber surface, is evaporated into the plasma by the radiation of arc discharge. Since this cesium ionization is accelerated in the long-pulse arc discharge, the volume effect of the cesium on the negative ion enhancement would be also considered.

In order to clarify the influence of the long-pulse arc discharge on the H^- ion beam properties, the pre-arc discharge time is varied. The pre-arc time is defined here as the

discharge time until the start of the negative ion extraction and acceleration, as shown in Fig. 7 (a). The I_{H^-}, I_{ext}, I_{acc} and the 1/e-half width of the vertical profile of the H^- ion beam are shown in Fig. 7 (b), as a function of the pre-arc discharge time. The arc power is 50 kW and the pulse length is 0.6 s. The currents and the 1/e-half width show almost no change for the pre-arc time variation. The plasma grid temperature is raised over 30 ℃ for a pre-arc time of 14 s, as shown in Fig. 7 (c), and the temperature variation during the long-pulse arc discharge has no influence on the beam properties. The steady negative ion beam is expected to be obtained for a long pulse duration from these results.

The H^- ion current, I_{H^-}, as a function of the arc power is shown in Fig. 8, in a long-pulse arc discharge. The beam pulse length is 0.6 s. The shaped aperture extraction grid shown in Fig. 2 (b) is used in this case. The I_{H^-} increases proportionally to the arc power. The ratio of the H^- ion current density at the plasma grid aperture to the arc power, i.e., the arc efficiency, is about 0.29 mA cm^{-2}/kW. The arc efficiency in a short-pulse arc discharge was about 0.20 mA cm^{-2}/kW, where the total H^- ion current was 16.2 A with a plasma grid of 25 cm $\times$ 50 cm in area. It is found that the negative ion production efficiency is improved by making the arc discharge longer and stable. The long-pulse stable arc discharge leads to a uniform cesium distribution in the arc chamber and the optimum condition in the cesium-seeded operation would be easily obtained. The equivalent thermal load currents to the extraction grid and the acceleration grid, I_{eg} and I_{gg}, respectively, are also shown in Fig. 8. The I_{eg} and the I_{gg} are obtained by dividing the thermal loads of the extraction grid and the acceleration grid by the extraction voltage and the acceleration voltage, respectively. The thermal load of grid is required to be low for the long-pulse negative ion beam production. The I_{eg} and the I_{gg} are about 20 % and about 13 % of the I_{H^-}, respectively. The grounded grid thermal load is mainly due to the impinging of the accelerated electrons produced by the negative ion stripping during the acceleration in the case of the shaped aperture extraction grid.[13] Thus, the reduction of the operational gas pressure is quite important for a high-power long-pulse operation. The thermal load of the extraction grid is small enough for the long-pulse operation.

C. Long-pulse negative ion beam production

The long-pulse operation up to 10 s has been performed with the calorimeter arrays removed. Figure 9 shows an example of the time evolution of the extraction voltage and current, the acceleration voltage and current, the arc current, and the water temperature rises of the extraction grid, the grounded grid and the neutral beam dump. The H^- ion beam power is

300 kW (83 keV - 3.6 A). Since the ion deflecting magnet is off. the all beams are incident on the neutral beam dump located 13 m downstream. The power supply currents are stationary for 10 s. The temperature rise of the grounded grid and the neutral beam dump becomes almost steady while that of the extraction grid does not reach a steady-state because of the larger thermal capacity than that of the grounded grid.

The thermal loads of the neutral beam dump, the extraction grid and the grounded grid are shown in Fig. 10, as a function of the beam pulse length. Since these thermal loads increase proportionally to the beam pulse length, it is thought that the beam properties does not change for 10 s. In Fig. 10, a high-power negative ion beam of 330 kW (91 keV-3.6 A) is produced for 10 s. The current density at the plasma grid is 21 mA/cm^2 and the negative ion power density at the grounded grid is 1.9 kW/cm^2. The water temperature rise of the grounded grid was higher than 20 ℃ in this case, and, therefore, the higher-power long-pulse experiment was not performed. The water flow rate is about 1.8 l/min per one cooling tube of 2.4 mm in inner diameter. The cooling ability would be improved four times by making the tube diameter larger, raising the supply water pressure and using cooler inlet water to enlarge the allowance of the water temperature rise. By this improvement, a high-power negative ion beam with a current density of 40 mA/cm^2 and an energy of 180 keV could be produced for 10 s, which satisfies the LHD-NBI specification. However, it is more important to lower the operational gas pressure for the reduction of the stripping loss of H^- ions, which leads to a decrease in the grounded grid thermal load.

D. Neutralization efficiency

The neutralization efficiency of the accelerated negative ions was measured before with the thermocouples attached on the neutral beam dump.[14] Since the beam pulse length was short below 0.3 s at that time, the neutralization efficiency was estimated from the ratio of the temperature rise of the thermocouples with the ion deflecting magnet operated to that without it. This is because the heat load to the actively cooled beam dumps was too small to measure the cooling water temperature rise. As shown in Fig. 9, the long-pulse negative ion beam raises the cooling water temperature of the neutral beam dump. Therefore, the neutralization efficiency of the accelerated negative ions can be estimated including the residual positive and negative ion ratios with the water-calorimetry.

Figure 11 (a) shows an example of the time evolution of the water temperature rises of the neutral, the positive ion and the negative ion beam dumps located 13 m downstream from the ion source. The beam energy is 91 keV and the negative ion beam power is about 320 kW.

The hydrogen gas is fed into the ion source vacuum vessel and the gas pressure in the vessel is 1.3×10^{-4} Torr in this case. Since the cryopump is operated only in the ion source vacuum vessel, the gas pressure is thought to be almost constant along the negative ion beam path to the beam dumps. As shown in Fig. 11 (a), stable temperature rise is observed for each beam dump, although the time response of the temperature rise is slow due to thick sheath covering the thermocouples inserted into the pressurized cooling water. The neutral, the positive ion and the negative ion ratios in the beam are estimated from the heat load of the beam dumps, and the results are shown in Fig. 11 (b), as a function of the gas pressure in the ion source vacuum vessel. The corresponding gas thickness is shown at the upper axis in the figure. The beam energy is 91 keV and the beam power is about 320 kW. The calculation result using the cross sections is also indicated with small closed symbols. It is found that the experimental result of the neutralization efficiency agrees well with the calculation result including the residual ion ratios. While the neutral ratio is kept at around 60 % in a relatively wide range of gas thickness, the residual ion ratios are sensitive to the gas thickness. From a point of view of the beam dump design, the negative-ion-based injector should be operated at a gas thickness giving the equal ratios of the residual positive and negative ions.

In conclusion, a long-pulse operation of a high-power large negative ion source was performed using a shaped aperture extraction grid, and the negative ion beam power of 330 kW was produced stably for 10 s from an ion source area of 25 cm $\times$ 26 cm. By improving the cooling ability of the grounded grid, the high-power long-pulse injection for 10 s will be possible in the LHD-NBI system.

REFERENCES

1 R. Aymar, V. Chuyanov, M. Huguet, R. Parker, Y. Shimomura, and the ITER Joint Central Team and Home Teams, *Proc. of the 16th IAEA Fusion Energy Conference, Montreal, Canada, 1996*, IAEA-CN-64/O1-1.

2 R. S. Hemsworth, J.-H. Feist, M. Hanada, B. Heinemann, T. Inoue, E. Kussel, A. Krylov, P. Lotte, K. Miyamoto, N. Miyamoto, D. Murdoch, A. Nagase, Y. Ohara, Y. Okumura, J. Pamela, A. Panasenkov, K. Shibata, M. Tanii, and M. Watson, Rev. Sci. Instrum. **67**, 1120 (1996).

3 Y. Okumura, Y. Fujiwara, T. Inoue, K. Miyamoto, N. Miyamoto, A. Nagase, Y. Ohara, and K. Watanabe, Rev. Sci. Instrum. **67**, 1092 (1996).

4 Y. Takeiri, O. Kaneko, Y. Oka, K. Tsumori, E. Asano, R. Akiyama, T. Kawamoto, T. Kuroda, and A. Ando, Rev. Sci. Instrum. **67**, 1021 (1996).

5 A. Simonin, J. Bucalossi, C. Desgranges, M. Fumelli, C. Jacquot, P. Massmann, J. Pamela, D. Riz, and R. Trainham, Rev. Sci. Instrum. **67**, 1102 (1996).

6 Y. Takeiri, A. Ando, O. Kaneko, Y. Oka, K. Tsumori, R. Akiyama, E. Asano, T. Kawamoto, T. Kuroda, M. Tanaka and H. Kawakami, Rev. Sci. Instrum. **66**, 2541 (1995).

7 K. Miyamoto, N. Akino, T. Aoyagi, N. Ebisawa, Y. Fujiwara, A. Honda, T. Inoue, T. Itoh, M. Kawai, M. Kazawa, J. Koizumi, M. Kuriyama, N. Miyamoto, K. Mogaki, Y. Ohara, T. Ohga, K. Ohshima, Y. Okumura, H. Oohara, F. Satoh, K. Usui, K. Watanabe, M. Yamamoto, T. Yamazaki, *Proc. of the 16th IAEA Fusion Energy Conference, Montreal, Canada, 1996*, IAEA-CN-64/GP-10.

8 K. Ushigusa and The JT-60 Team, *Proc. of the 16th IAEA Fusion Energy Conference, Montreal, Canada, 1996*, IAEA-CN-64/O1-3.

9 A. Iiyoshi, M. Fujiwara, O. Motojima, N. Ohyabu and K. Yamazaki, Fusion Technology **17**, 169 (1990).

10 Y. Takeiri, O. Kaneko, F. Sano, A. Ando, Y. Oka, K. Hanatani, T. Obiki and T. Kuroda, *Proc. of the first Int. Toki Conf. on Plasma Physics and Controlled Nuclear Fusion, Toki, Japan, 1989*, p. 272.

11 O. Kaneko, Y. Takeiri, K. Tsumori, Y. Oka, M. Osakabe, R. Akiyama, T. Kawamoto, E. Asano, and T. Kuroda, *Proc. of the 16th IAEA Fusion Energy Conference, Montreal, Canada, 1996*, IAEA-CN-64/GP-9.

12 Y. Okumura, M. Hanada, T. Inoue, M. Mizuno, Y. Ohara, Y. Suzuki, H. Tanaka, M. Tanaka, and K. Watanabe, Rev. Sci. Instrum. **63**, 2708 (1992).

13 Y. Takeiri, Y. Oka, M. Osakabe, K. Tsumori, O. Kaneko, T. Takanashi, E. Asano, T.

Kawamoto, R. Akiyama, and T. Kuroda, submitted.

14 Y. Takeiri, A. Ando, O. Kaneko, Y. Oka, K. Tsumori, R. Akiyama, E. Asano, T. Kawamoto, M. Tanaka and T. Kuroda, J. Plasma Fusion Res. **71**, 605 (1995).

15 Y. Takeiri, O. Kaneko, Y. Oka, K. Tsumori, E. Asano, R. Akiyama, T. Kawamoto, T. Kuroda, and A. Ando, Rev. Sci. Instrum. **66**, 5236 (1995).

16 O. Kaneko, A. Ando, Y. Oka, Y. Takeiri, K. Tsumori, R. Akiyama, T. Kawamoto, T. Kurata, K. Mineo and T. Kuroda, *Proc. of the 17th Symp.on Fusion Technology, Rome, 1992*, p. 544.

17 Y. Takeiri, A. Ando, O. Kaneko, Y. Oka, K. Tsumori, R. Akiyama, T. Kawamoto and T. Kuroda, *Proc. of the 6th Int. Symp. on Production and Neutralization of Negative Ions and Beams, Upton, NY, 1992*, AIP Conf. Proc. No. 287, p. 869.

18 Y. Okumura, Y. Fujiwara, A. Honda, T. Inoue, M. Kuriyama, K. Miyamoto, N. Miyamoto, K. Mogaki, A. Nagase, Y. Ohara, K. Usui, and K. Watanabe, Rev. Sci. Instrum. **67**, 1018 (1996).

19 Y. Okumura, M. Hanada, T. Inoue, H. Kojima, Y. Matsuda, Y. Ohara, M. Seki and K. Watanabe, *Proc. of the 5th Int. Symp. on the Production and Neutralization of Negative Ions and Beams, Brookhaven, 1990*, AIP Conf. Proc. No. 210, p. 169.

20 A. Ando, K. Tsumori, Y. Takeiri, O. Kaneko, Y. Oka, T. Okumura, H. Kojima, Y. Yamashita, R. Akiyama, T. Kawamoto, K. Mineo, T. Kurata and T. Kuroda, *Proc. of the 6th Int. Symp. on Production and Neutralization of Negative Ions and Beams, Upton, NY, 1992*, AIP Conf. Proc. No. 287, p. 339.

FIGURE CAPTIONS

Fig. 1 Schematic diagram of an external filter type large hydrogen negative ion source.

Fig. 2 Three-grid single-stage accelerators (a) with a straight aperture extraction grid and (b) with a shaped aperture extraction grid.

Fig. 3 Schematic diagram of a negative-ion-based NBI teststand.

Fig. 4 (a) Arrangement of the filament and arc power supplies. The filament power supply provides eight electrically isolated outputs, and a variable resistance is inserted between each isolated filament power supply output and the arc power supply. (b) An example of the time evolution of the individual arc current distribution.

Fig. 5 H^- ion current, I_{H^-}, the extraction current, I_{ext}, the acceleration current, I_{acc}, and the FWHM of the vertical profile of the H^- ion beam as a function of the beam pulse length in a long-pulse arc discharge. The arc power is 60 kW.

Fig. 6 H^- ion current, I_{H^-}, the extraction current, I_{ext}, the acceleration current, I_{acc}, and the 1/e-half width of the vertical profile of the H^- ion beam as a function of the plasma grid temperature in a long-pulse arc discharge. The arc power is 67 kW and the beam pulse length is 0.6 s.

Fig. 7 (a) Time evolution of the arc current. The pre-arc time is defined as the discharge time before the beam pulse. (b) The H^- ion current, I_{H^-}, the extraction current, I_{ext}, the acceleration current, I_{acc}, and the 1/e-half width of the vertical profile of the H^- ion beam, and (c) the plasma grid temperature rise as a function of the pre-arc time. The arc power is 50 kW and the beam pulse length is 0.6 s. The plasma grid temperature at the start of the arc discharge is 220 ℃.

Fig. 8 H^- ion current, I_{H^-}, and the equivalent thermal load currents to the extraction grid, I_{eg}, and the acceleration grid, I_{gg}, as a function of the arc power in a long-pulse arc discharge. The beam pulse length is 0.6 s.

Fig. 9 Example of the time evolution of the extraction voltage and current, the acceleration voltage and current, the arc current, and the water temperature rises of the extraction grid, the grounded grid and the neutral beam dump. The H^- ion beam power is 300 kW (83 keV - 3.6 A). The ion deflecting magnet is off.

Fig. 10 Thermal loads of the neutral beam dump, the extraction grid and the grounded grid as a function of the beam pulse length. The H^- ion beam power is 330 kW (91 keV - 3.6 A).

Fig. 11 (a) Example of the time evolution of the water temperature rises of the neutral, the

positive ion and the negative ion beam dumps at a gas pressure in the ion source vacuum vessel of 1.3×10^{-4} Torr, and (b) the neutral, the positive ion and the negative ion ratios in the beam as a function of the gas pressure in the ion source vacuum vessel. The H^- ion beam power is about 320 kW and the beam energy is 91 keV. The corresponding gas thickness to the gas pressure in the ion source vacuum vessel is shown at the upper axis in (b). The calculation result using the cross sections is also indicated with small closed symbols in (b).

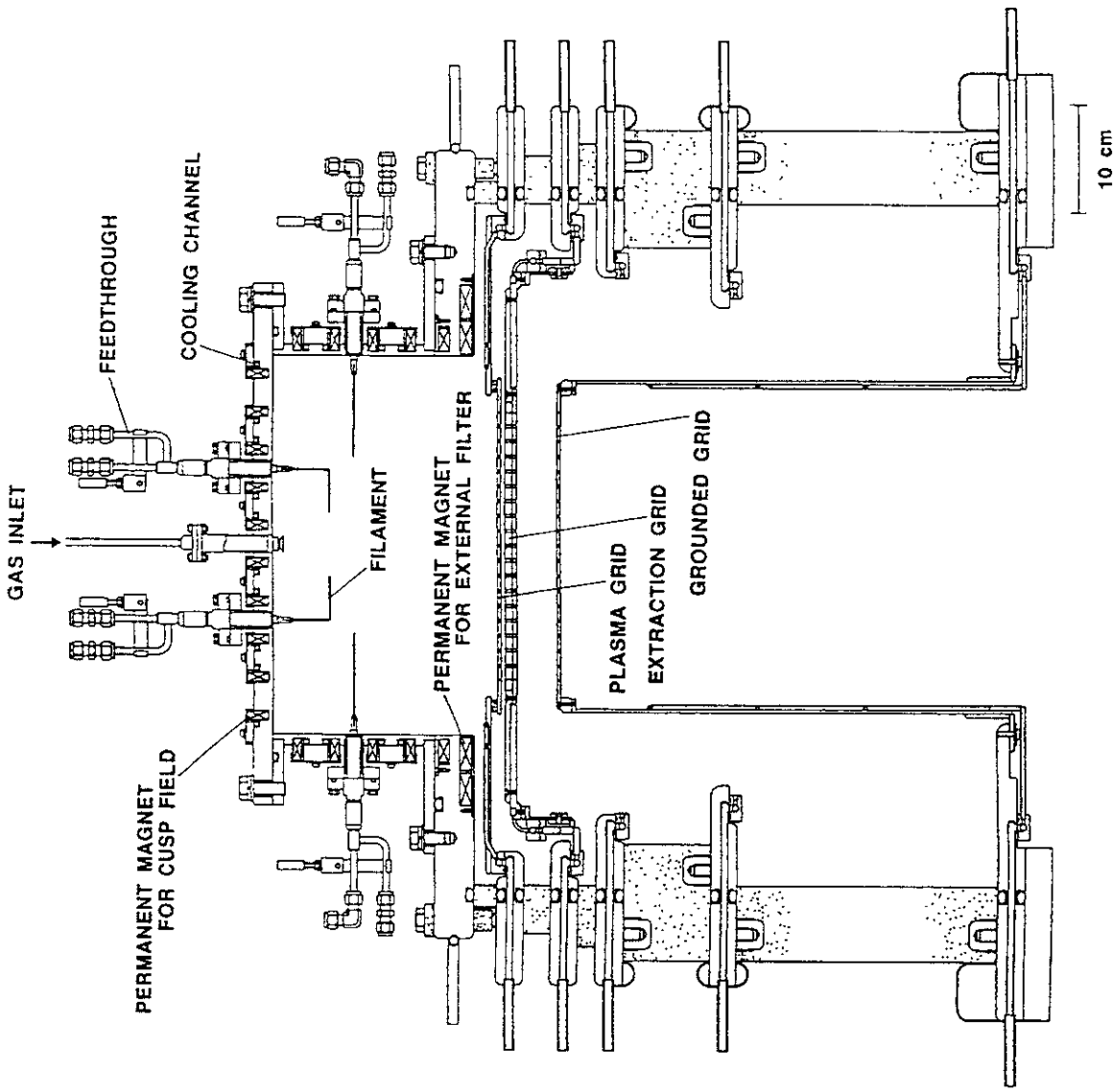

Figure 1
Y. Takeiri, *et al.*

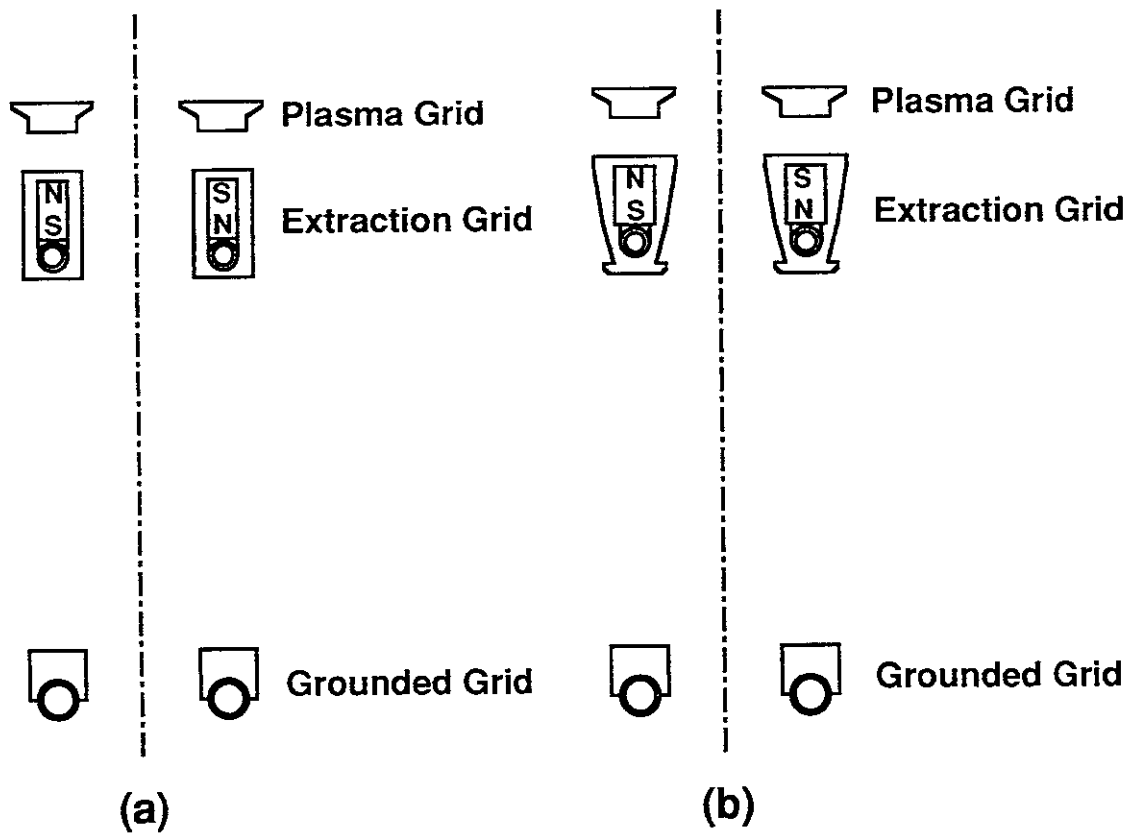

Figure 2
Y. Takeiri, *et al.*

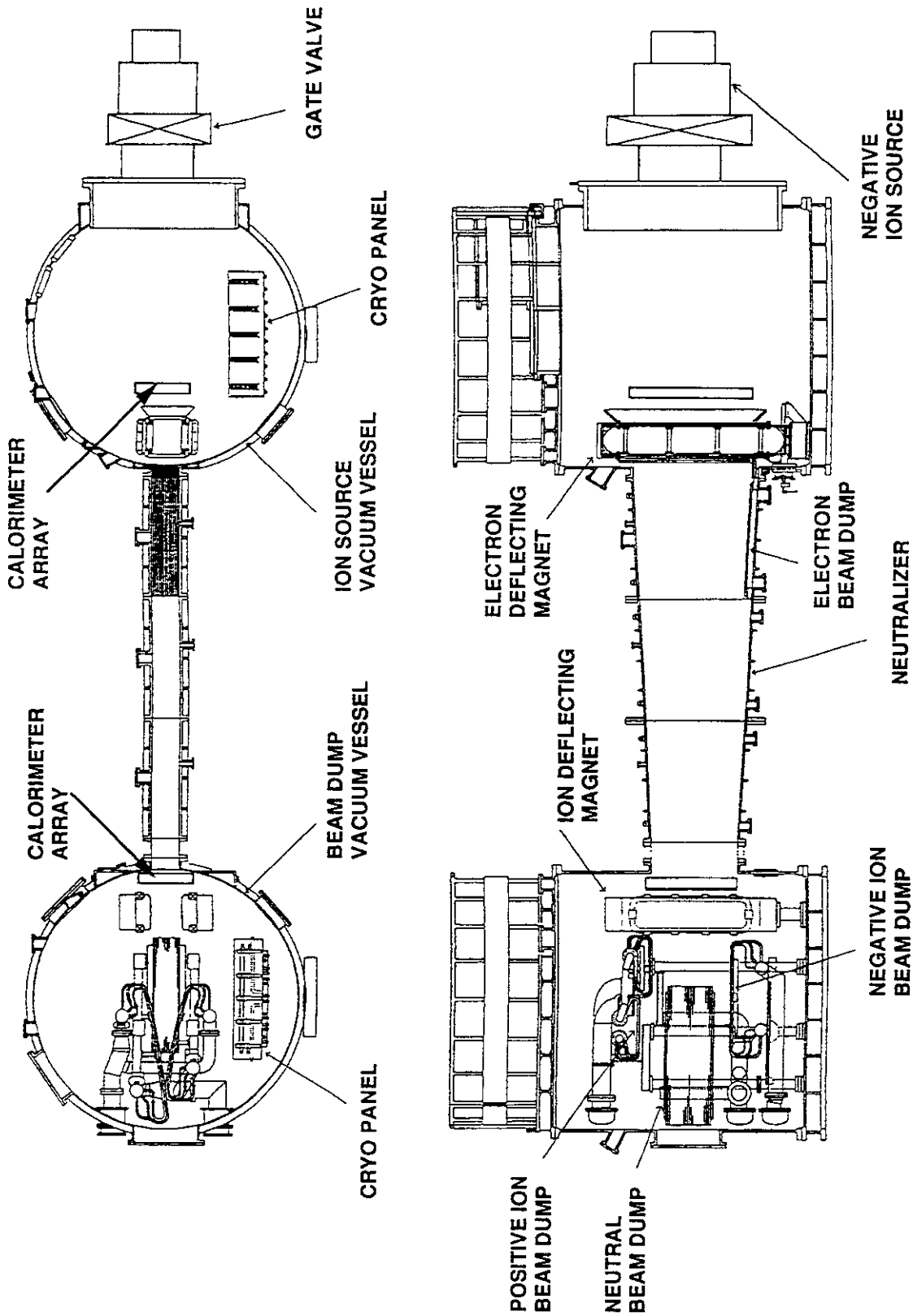

Figure 3
Y. Takeiri, *et al.*

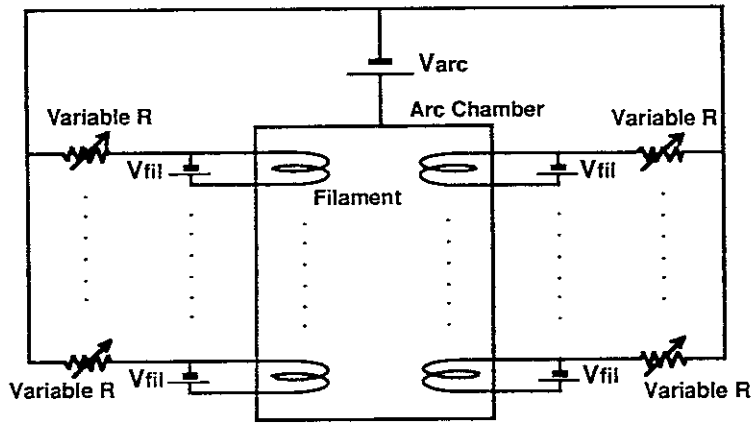

(a)

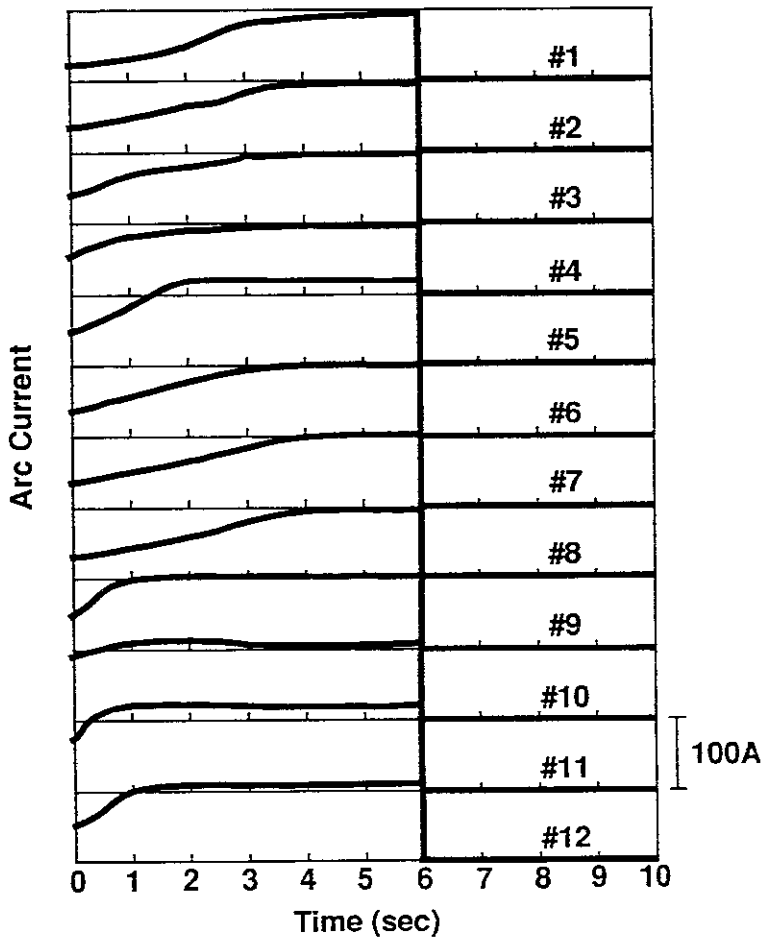

(b)

Figure 4
Y. Takeiri, *et*

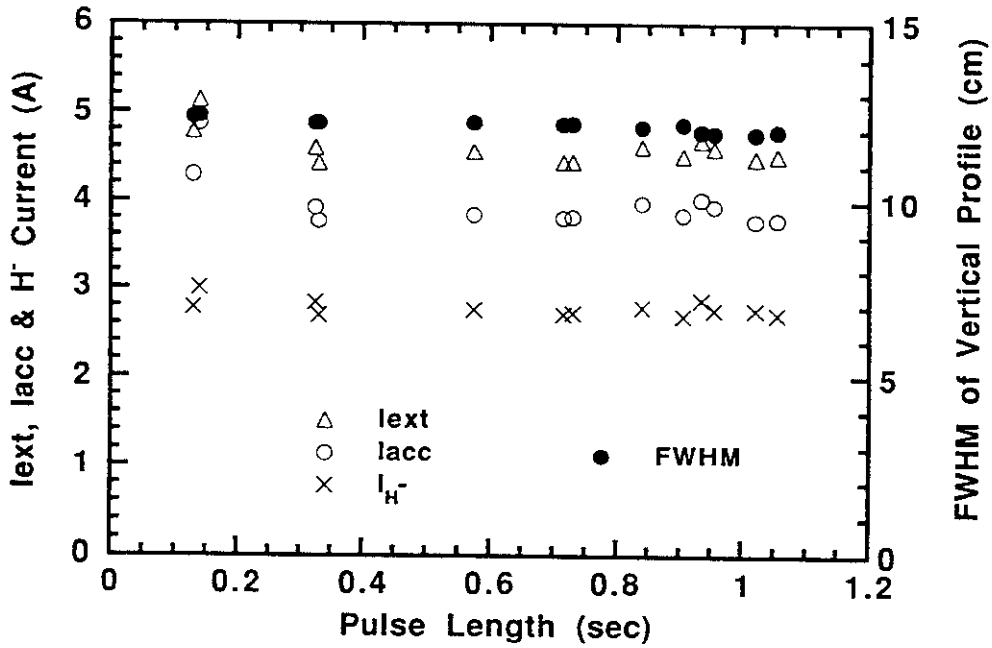

Figure 5
Y. Takeiri, *et al.*

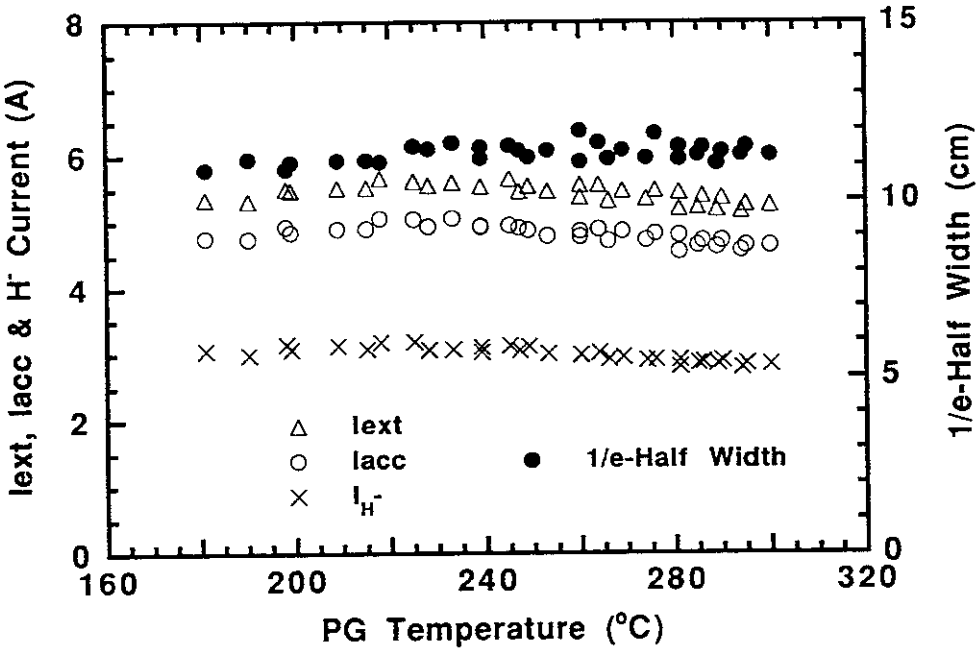

Figure 6
Y. Takeiri, *et al.*

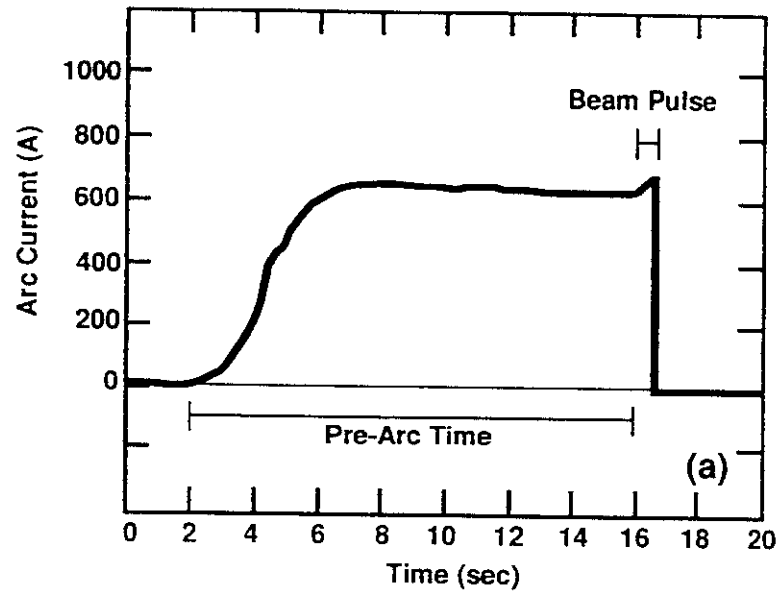

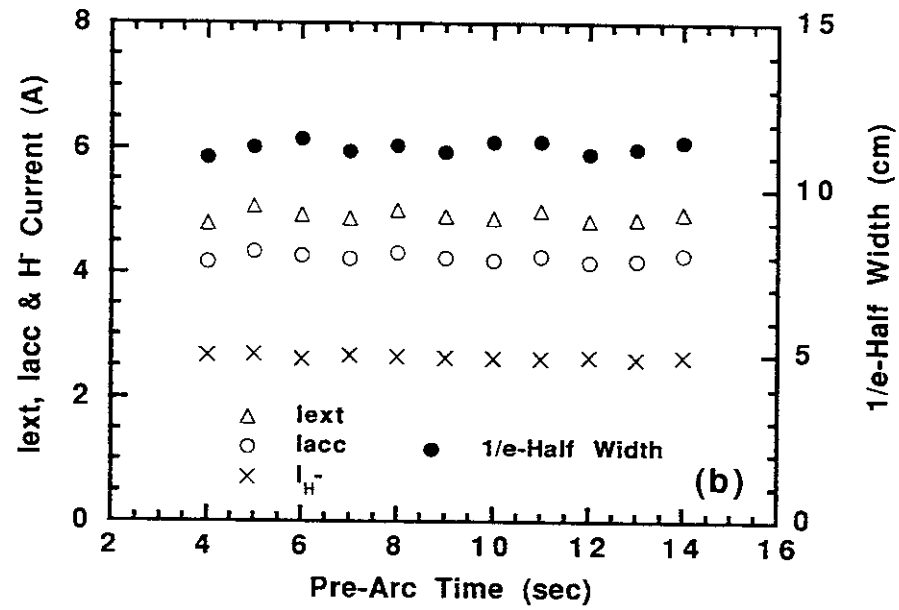

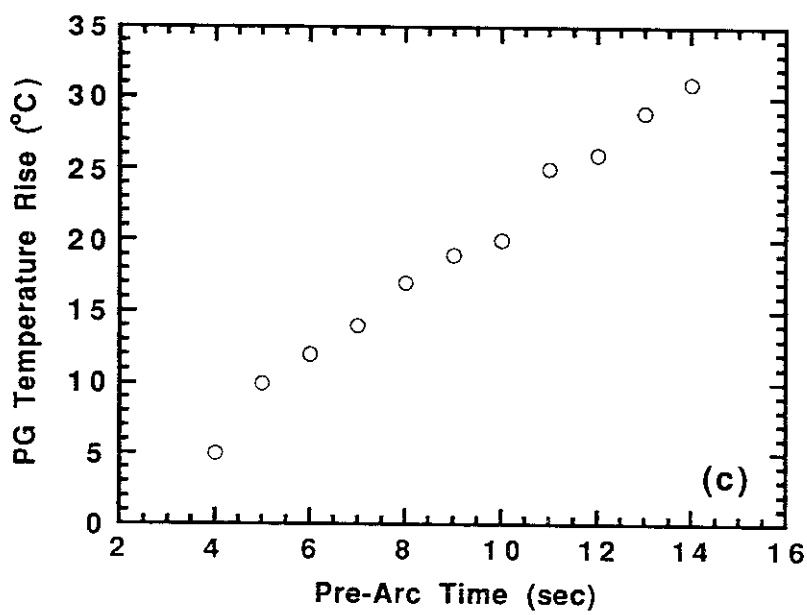

Figure 7
Y. Takeiri, *et al.*

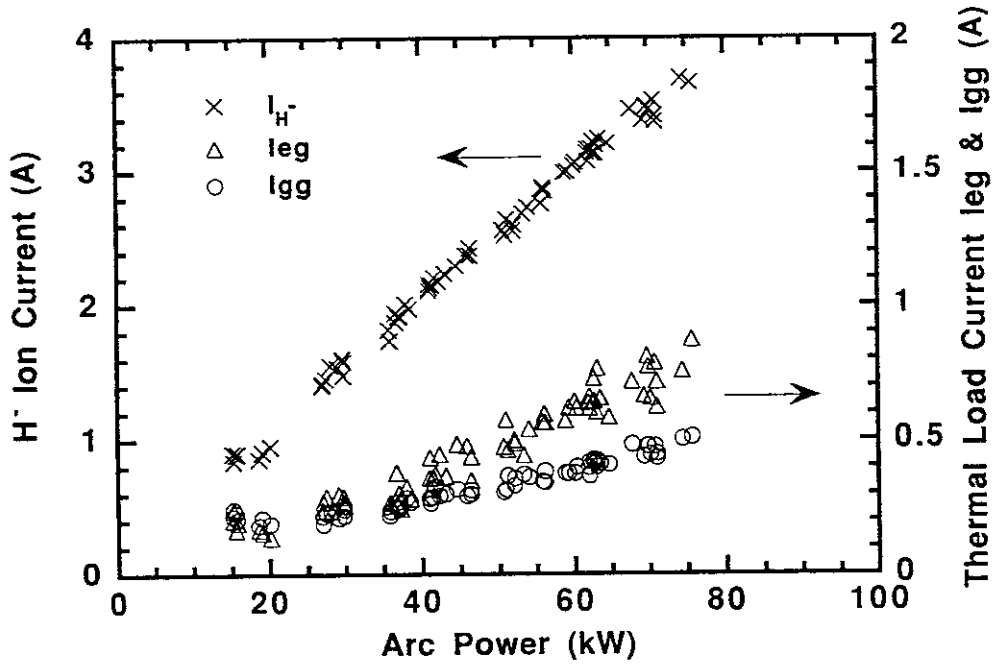

Figure 8
Y. Takeiri, *et al.*

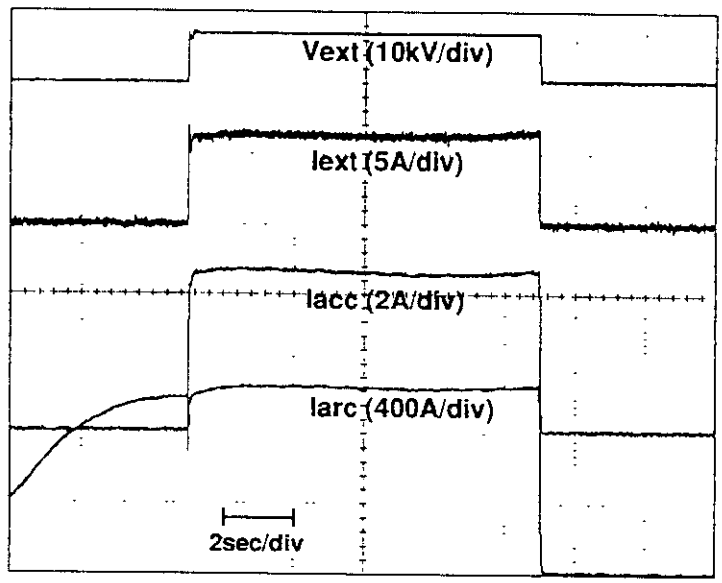

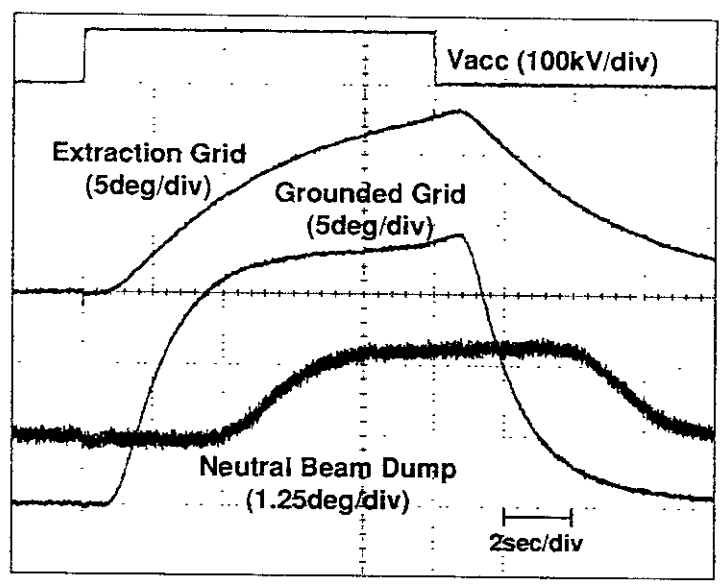

Figure 9
Y. Takeiri, *et al.*

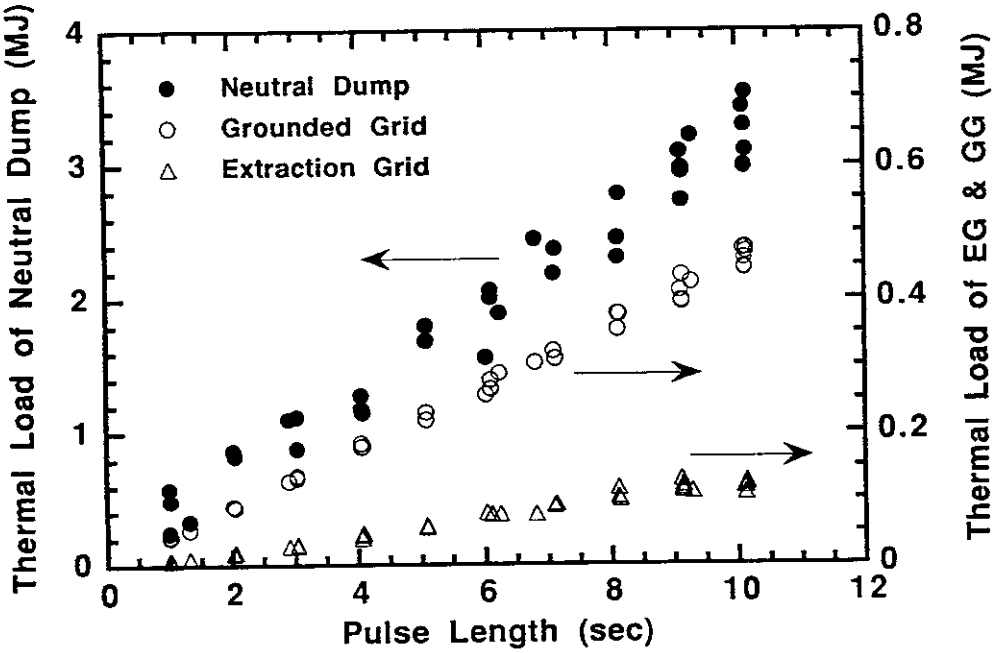

Figure 10
Y. Takeiri, *et al.*

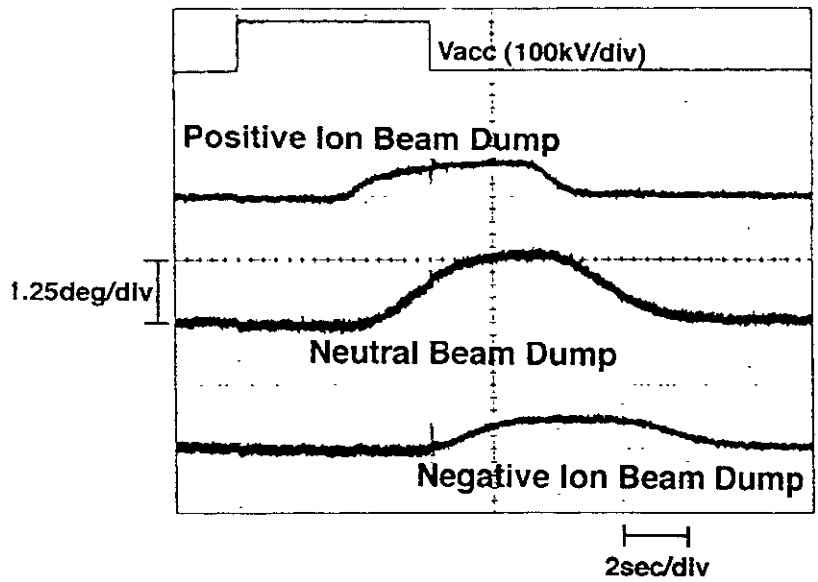

(a)

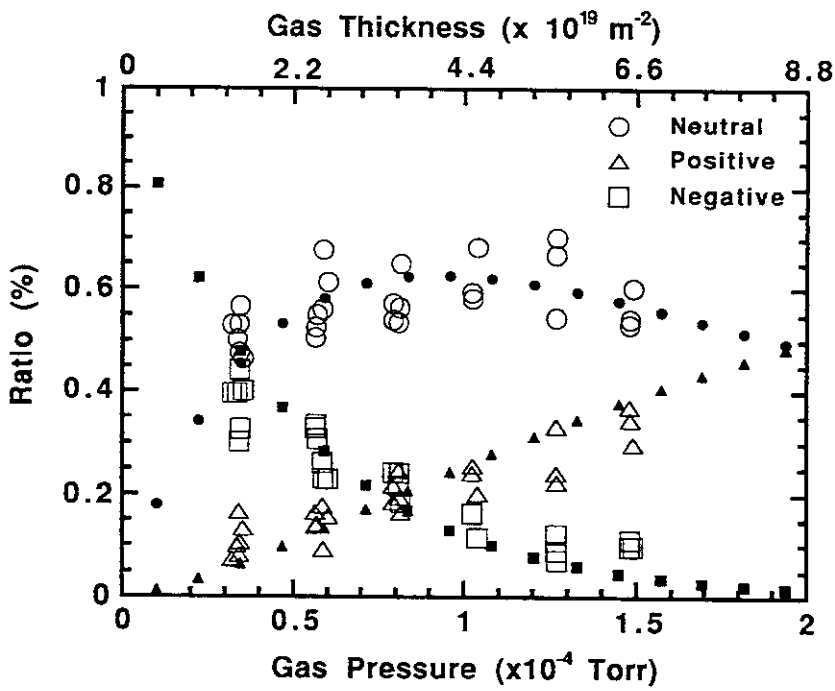

(b)

Figure 11
Y. Takeiri, *et al.*

Recent Issues of NIFS Series

NIFS-437 T. Morisaki, A. Komori, R. Akiyama, H. Idei, H. Iguchi, N. Inoue, Y. Kawai, S. Kubo, S. Masuzaki, K. Matsuoka, T. Minami, S. Morita, N. Noda, N. Ohyabu, S. Okamura, M. Osakabe, H. Suzuki, K. Tanaka, C. Takahashi, H. Yamada, I. Yamada and O. Motojima,
Experimental Study of Edge Plasma Structure in Various Discharges on Compact Helical System; Aug. 1996

NIFS-438 A. Komori, N. Ohyabu, S. Masuzaki, T. Morisaki, H. Suzuki, C. Takahashi, S. Sakakibara, K. Watanabe, T. Watanabe, T. Minami, S. Morita, K. Tanaka, S. Ohdachi, S. Kubo, N. Inoue, H. Yamada, K. Nishimura, S. Okamura, K. Matsuoka, O. Motojima, M. Fujiwara, A. Iiyoshi, C. C. Klepper, J.F. Lyon, A.C. England, D.E. Greenwood, D.K. Lee, D.R. Overbey, J.A. Rome, D.E. Schechter and C.T. Wilson,
Edge Plasma Control by a Local Island Divertor in the Compact Helical System; Sep. 1996 (IAEA-CN-64/C1-2)

NIFS-439 K. Ida, K. Kondo, K. Nagaski T. Hamada, H. Zushi, S. Hidekuma, F. Sano, T. Mizuuchi, H. Okada, S. Besshou, H. Funaba, Y. Kurimoto, K. Watanabe and T. Obiki,
Dynamics of Ion Temperature in Heliotron-E; Sep. 1996 (IAEA-CN-64/CP-5)

NIFS-440 S. Morita, H. Idei, H. Iguchi, S. Kubo, K. Matsuoka, T. Minami, S. Okamura, T. Ozaki, K. Tanaka, K. Toi, R. Akiyama, A. Ejiri, A. Fujisawa, M. Fujiwara, M. Goto, K. Ida, N. Inoue, A. Komori, R. Kumazawa, S. Masuzaki, T. Morisaki, S. Muto, K. Narihara, K. Nishimura, I. Nomura, S. Ohdachi, M.. Osakabe, A. Sagara, Y. Shirai, H. Suzuki, C. Takahashi, K. Tsumori, T. Watari, H. Yamada and I. Yamada,
A Study on Density Profile and Density Limit of NBI Plasmas in CHS; Sep. 1996 (IAEA-CN-64/CP-3)

NIFS-441 O. Kaneko, Y. Takeiri, K. Tsumori, Y. Oka, M. Osakabe, R. Akiyama, T. Kawamoto, E. Asano and T. Kuroda,
Development of Negative-Ion-Based Neutral Beam Injector for the Large Helical Device; Sep. 1996 (IAEA-CN-64/GP-9)

NIFS-442 K. Toi, K.N. Sato, Y. Hamada, S. Ohdachi, H. Sakakita, A. Nishizawa, A. Ejiri, K. Narihara, H. Kuramoto, Y. Kawasumi, S. Kubo, T. Seki, K. Kitachi, J. Xu, K. Ida, K. Kawahata, I. Nomura, K. Adachi, R. Akiyama, A. Fujisawa, J. Fujita, N. Hiraki, S. Hidekuma, S. Hirokura, H. Idei, T. Ido, H. Iguchi, K. Iwasaki, M. Isobe, O. Kaneko, Y. Kano, M. Kojima, J. Koog, R. Kumazawa, T. Kuroda, J. Li, R. Liang, T. Minami, S. Morita, K. Ohkubo, Y. Oka, S. Okajima, M. Osakabe, Y. Sakawa, M. Sasao, K. Sato, T. Shimpo, T. Shoji, H. Sugai, T. Watari, I. Yamada and K. Yamauti,
Studies of Perturbative Plasma Transport, Ice Pellet Ablation and Sawtooth Phenomena in the JIPP T-IIU Tokamak; Sep. 1996 (IAEA-CN-64/A6-5)

NIFS-443 Y. Todo, T. Sato and The Complexity Simulation Group,

Vlasov-MHD and Particle-MHD Simulations of the Toroidal Alfvén Eigenmode; Sep. 1996 (IAEA-CN-64/D2-3)

NIFS-444 A. Fujisawa, S. Kubo, H. Iguchi, H. Idei, T. Minami, H. Sanuki, K. Itoh, S. Okamura, K. Matsuoka, K. Tanaka, S. Lee, M. Kojima, T.P. Crowley, Y. Hamada, M. Iwase, H. Nagasaki, H. Suzuki, N. Inoue, R. Akiyama, M. Osakabe, S. Morita, C. Takahashi, S. Muto, A. Ejiri, K. Ida, S. Nishimura, K. Narihara, I. Yamada, K. Toi, S. Ohdachi, T. Ozaki, A. Komori, K. Nishimura, S. Hidekuma, K. Ohkubo, D.A. Rasmussen, J.B. Wilgen, M. Murakami, T. Watari and M. Fujiwara,
An Experimental Study of Plasma Confinement and Heating Efficiency through the Potential Profile Measurements with a Heavy Ion Beam Probe in the Compact Helical System; Sep. 1996 (IAEA-CN-64/C1-5)

NIFS-445 O. Motojima, N. Yanagi, S. Imagawa, K. Takahata, S. Yamada, A. Iwamoto, H. Chikaraishi, S. Kitagawa, R. Maekawa, S. Masuzaki, T. Mito, T. Morisaki, A. Nishimura, S. Sakakibara, S. Satoh, T. Satow, H. Tamura, S. Tanahashi, K. Watanabe, S. Yamaguchi, J. Yamamoto, M.Fujiwara and A. Iiyoshi,
Superconducting Magnet Design and Construction of LHD; Sep. 1996 (IAEA-CN-64/G2-4)

NIFS-446 S. Murakami, N. Nakajima, S. Okamura, M. Okamoto and U. Gasparino,
Orbit Effects of Energetic Particles on the Reachable β–Value and the Radial Electric Field in NBI and ECR Heated Heliotron Plasmas; Sep. 1996 (IAEA-CN-64/CP -6) Sep. 1996

NIFS-447 K. Yamazaki, A. Sagara, O. Motojima, M. Fujiwara, T. Amano, H. Chikaraishi, S. Imagawa, T. Muroga, N. Noda, N. Ohyabu, T. Satow, J.F. Wang, K.Y. Watanabe, J. Yamamoto , H. Yamanishi, A. Kohyama, H. Matsui, O. Mitarai, T. Noda, A.A. Shishkin, S. Tanaka and T. Terai
Design Assessment of Heliotron Reactor; Sep. 1996 (IAEA-CN-64/G1-5)

NIFS-448 M. Ozaki, T. Sato and the Complexity Simulation Group,
Interactions of Convecting Magnetic Loops and Arcades; Sep. 1996

NIFS-449 T. Aoki,
Interpolated Differential Operator (IDO) Scheme for Solving Partial Differential Equations; Sep. 1996

NIFS-450 D. Biskamp and T. Sato,
Partial Reconnection in the Sawtooth Collapse; Sep. 1996

NIFS-451 J. Li, X. Gong, L. Luo, F.X. Yin, N. Noda, B. Wan, W. Xu, X. Gao, F. Yin, J.G. Jiang, Z. Wu., J.Y. Zhao, M. Wu, S. Liu and Y. Han,
Effects of High Z Probe on Plasma Behavior in HT-6M Tokamak; Sep. 1996

NIFS-452 N. Nakajima, K. Ichiguchi, M. Okamoto and R.L. Dewar,
Ballooning Modes in Heliotrons/Torsatrons; Sep. 1996 (IAEA-CN-64/D3-6)

NIFS-453 A. Iiyoshi,

Overview of Helical Systems; Sep. 1996 (IAEA-CN-64/O1-7)

NIFS-454 S. Saito, Y. Nomura, K. Hirose and Y.H. Ichikawa,
Separatrix Reconnection and Periodic Orbit Annihilation in the Harper Map; Oct. 1996

NIFS-455 K. Ichiguchi, N. Nakajima and M. Okamoto,
Topics on MHD Equilibrium and Stability in Heliotron / Torsatron; Oct. 1996

NIFS-456 G. Kawahara, S. Kida, M. Tanaka and S. Yanase,
Wrap, Tilt and Stretch of Vorticity Lines around a Strong Straight Vortex Tube in a Simple Shear Flow; Oct. 1996

NIFS-457 K. Itoh, S.-I. Itoh, A. Fukuyama and M. Yagi,
Turbulent Transport and Structural Transition in Confined Plasmas; Oct. 1996

NIFS-458 A. Kageyama and T. Sato,
Generation Mechanism of a Dipole Field by a Magnetohydrodynamic Dynamo; Oct. 1996

NIFS-459 K. Araki, J. Mizushima and S. Yanase,
The Non-axisymmetric Instability of the Wide-Gap Spherical Couette Flow; Oct. 1996

NIFS-460 Y. Hamada, A. Fujisawa, H. Iguchi, A. Nishizawa and Y. Kawasumi,
A Tandem Parallel Plate Analyzer; Nov. 1996

NIFS-461 Y. Hamada, A. Nishizawa, Y. Kawasumi, A. Fujisawa, K. Narihara, K. Ida, A. Ejiri, S. Ohdachi, K. Kawahata, K. Toi, K. Sato, T. Seki, H. Iguchi, K. Adachi, S. Hidekuma, S.Hirokura, K. Iwasaki, T. Ido, M. Kojima, J. Koong, R. Kumazawa, H. Kuramoto, T. Minami, I. Nomura, H. Sakakita, M. Sasao, K.N. Sato, T. Tsuzuki, J. Xu, I. Yamada and T. Watari,
Density Fluctuation in JIPP T-IIU Tokamak Plasmas Measured by a Heavy Ion Beam Probe; Nov. 1996

NIFS-462 N. Katsuragawa, H. Hojo and A. Mase,
Simulation Study on Cross Polarization Scattering of Ultrashort-Pulse Electromagnetic Waves; Nov. 1996

NIFS-463 V. Voitsenya, V. Konovalov, O. Motojima, K. Narihara, M. Becker and B. Schunke,
Evaluations of Different Metals for Manufacturing Mirrors of Thomson Scattering System for the LHD Divertor Plasma; Nov. 1996

NIFS-464 M. Pereyaslavets, M. Sato, T. Shimozuma, Y. Takita, H. Idei, S. Kubo, K. Ohkubo and K. Hayashi,
Development and Simulation of RF Components for High Power Millimeter Wave Gyrotrons; Nov. 1997

NIFS-465 V.S. Voitsenya, S. Masuzaki, O. Motojima, N. Noda and N. Ohyabu,
On the Use of CX Atom Analyzer for Study Characteristics of Ion Component in a LHD Divertor Plasma; Dec. 1996

NIFS-466 H. Miura and S. Kida,
Identification of Tubular Vortices in Complex Flows; Dec. 1996

NIFS-467 Y. Takeiri, Y. Oka, M. Osakabe, K. Tsumori, O. Kaneko, T. Takanashi, E. Asano, T. Kawamoto, R. Akiyama and T. Kuroda,
Suppression of Accelerated Electrons in a High-current Large Negative Ion Source; Dec. 1996

NIFS-468 A. Sagara, Y. Hasegawa, K. Tsuzuki, N. Inoue, H. Suzuki, T. Morisaki, N. Noda, O. Motojima, S. Okamura, K. Matsuoka, R. Akiyama, K. Ida, H. Idei, K. Iwasaki, S. Kubo, T. Minami, S. Morita, K. Narihara, T. Ozaki, K. Sato, C. Takahashi, K. Tanaka, K. Toi and I. Yamada,
Real Time Boronization Experiments in CHS and Scaling for LHD; Dec. 1996

NIFS-469 V.L. Vdovin, T.Watari and A. Fukuyama,
3D Maxwell-Vlasov Boundary Value Problem Solution in Stellarator Geometry in Ion Cyclotron Frequency Range (final report); Dec. 1996

NIFS-470 N. Nakajima, M. Yokoyama, M. Okamoto and J. Nührenberg,
Optimization of M=2 Stellarator; Dec. 1996

NIFS-471 A. Fujisawa, H. Iguchi, S. Lee and Y. Hamada,
Effects of Horizontal Injection Angle Displacements on Energy Measurements with Parallel Plate Energy Analyzer; Dec. 1996

NIFS-472 R. Kanno, N. Nakajima, H. Sugama, M. Okamoto and Y. Ogawa,
Effects of Finite-β and Radial Electric Fields on Neoclassical Transport in the Large Helical Device; Jan. 1997

NIFS-473 S. Murakami, N. Nakajima, U. Gasparino and M. Okamoto,
Simulation Study of Radial Electric Field in CHS and LHD; Jan. 1997

NIFS-474 K. Ohkubo, S. Kubo, H. Idei, M. Sato, T. Shimozuma and Y. Takita,
Coupling of Tilting Gaussian Beam with Hybrid Mode in the Corrugated Waveguide; Jan. 1997

NIFS-475 A. Fujisawa, H. Iguchi, S. Lee and Y. Hamada,
Consideration of Fluctuation in Secondary Beam Intensity of Heavy Ion Beam Prove Measurements; Jan. 1997

NIFS-476 Y. Takeiri, M. Osakabe, Y. Oka, K. Tsumori, O. Kaneko, T. Takanashi, E. Asano, T. Kawamoto, R. Akiyama and T. Kuroda,
Long-pulse Operation of a Cesium-Seeded High-Current Large Negative Ion Source; Jan. 1997